# Merged-beams energy-loss technique for electron-ion excitation: Absolute total cross sections for $O^{5+}(2s \rightarrow 2p)$

E. W. Bell, X. Q. Guo, J. L. Forand,* K. Rinn,† D. R. Swenson,‡ J. S. Thompson,§ and G. H. Dunn**
*Joint Institute for Laboratory Astrophysics, University of Colorado and National Institute of Standards and Technology, Boulder, Colorado 80309-0440*

M. E. Bannister, D. C. Gregory, and R. A. Phaneuf§
*Oak Ridge National Laboratory, Oak Ridge, Tennessee 37831*

A. C. H. Smith
*University College London, London, WC1E 6BT, United Kingdom*

A. Müller
*Institut für Strahlenphysik, Universität Stuttgart, D-70569 Stuttgart, Federal Republic of Germany*

C. A. Timmer and E. K. Wåhlin††
*Los Alamos National Laboratory, Los Alamos, New Mexico 87545*

B. D. DePaola
*Kansas State University, Manhattan, Kansas 66506*

D. S. Belić
*University of Beograd, P.O. Box 550, Beograd, Yugoslavia*
(Received 22 November 1993)

A merged-beams electron-energy-loss technique is described, by which absolute cross sections can be measured for near-threshold electron-impact excitation of multipy charged ions. Results are reported here for absolute total electron-impact excitation cross sections for the $O^{5+}(2s \rightarrow 2p)$ transition from below threshold to 1.6 eV above threshold. The experimental data are in good agremeent with a seven-state close-coupling calculation throughout the energy range of the experiment. Results agree with calculations showing that more than 90% of the electrons causing excitation are ejected in the backward direction in the center-of-mass frame. This backscattering is shown in both quantum-mechanical and semiclassical calculations. Evidence is observed for high-lying metastable autoionizing states with a lifetime of approximately 0.9 $\mu$s which are made to ionize by electron impact.

PACS number(s): 34.80.Kw, 35.80.+s

## I. INTRODUCTION

The description and modeling of natural and laboratory plasmas require quantitative information on the processes occurring within the plasma. The search for controlled nuclear fusion, intense activity in astrophysics, development of uv and x-ray lasers, and the study of planetary atmospheres and magnetospheres have particularly spurred both the calculation and measurement of atomic processes in plasmas. An especially important area, particularly in hot plasmas, is that of electron-ion collisions. This paper considers excitation of ions by electron impact.

Despite numerous theoretical calculations for electron-impact excitation of ions and an impressive number of experiments to measure excitation [1,2], there is still a serious need for experiments which test the ability to calculate such cross sections. The role of experiment must be that of testing whether theoretical calculations can quantitatively describe the atomic processes, because there is literally an infinity of transitions and species to contemplate, and lengthy and difficult experiments are possible for only a relatively few cases. Most data *must* be calculated.

Most experimental absolute total excitation cross sections have been measured using crossed beams of elec-

*Present address: Defense Research Establishment Valcartier, Courcelette, Quebec, Canada G0A 1RO.
†Present address: Wild Leitz, D-6330 Wetzlar, Germany.
‡Present address: Los Alamos National Laboratory, Los Alamos, NM 87545.
§Present address: Deparment of Physics, University of Nevada, Reno, NV 89557.
**Quantum Physics Division, National Institute of Standards and Technology, Boulder, CO 80303.
††Present address: Colutron Research Corp., Boulder, CO 80301.

 

trons and ions and detecting the fluorescence from the resulting excited state. This technique was primarily used for measurements on singly ionized target ions. Absolute total cross sections were, nevertheless, experimentally determined for the three multiply charged ion species of $C^{3+}$, $N^{4+}$, and $Al^{2+}$ [3] using the fluorescence method. However, because of the very low detection efficiency ($\approx 10^{-4}$), difficulty of dispersion and absolute radiometry of the uv and x-ray radiation, and low target densities, it became clear that this method would probably not serve for pursuing other multiply charged systems.

More recently, advances in technology have led to the invention of the electron-beam ion trap (EBIT) and the electron-beam ion source. These techniques can be used to study excitation by detecting x rays emitted by very highly charged ions and normalizing the data to theory. For example, the excitation of $Ba^{46+}$ has been measured using an EBIT [4]. This technique represents a breakthrough for studying very highly charged ions and is complementary to the method described in this paper. Even though results from the trap technique are not absolute and must be normalized to theory for (in the case of the EBIT) radiative recombination, it is generally thought that this introduces little uncertainty. Similarly, though one would like to have better electron-energy resolution than the tens of electron volts achieved in these experiments, there have nonetheless been observations of some resonances and the advantages substantially outweigh the drawbacks.

In order to rectify the problems intrinsic to the crossed-beams fluorescence approach, a merged-beams electron-energy-loss technique has been developed by us to measure absolute cross sections for excitation of multiply charged ions. The method involves collection and detection of nearly 100% of inelastically scattered and velocity-dispersed electrons from collinear beams with measured overlap so that the results are absolute in nature. We have previously reported results on $Si^{3+}$ [5] and $Ar^{7+}$ [6] using the method, which could not be adequately described in those short communications. Here we present results on the excitation $e+O^{5+}(2s\ ^2S_{1/2}) \rightarrow e+O^{5+}(2p\ ^2P_{1/2,3/2})$, and we describe the technique in some detail; still more detail is available elsewhere [2,7]. A closely related technique has also been developed and reported by Smith *et al.* [8], who have used it to study singly charged ions $Zn^+$ and $Mg^+$.

## II. MERGED-BEAMS TECHNIQUE

### A. General

The simple concept of colliding beams has been used for atomic collisions studies in both the crossed- and merged-beams configurations for more than sixty years [9]. In recent years, the merged beams method has been used effectively for electron-ion collisions related to recombination measurements [10,11]. Though merged beams are widely used at relativistic energies, the discussions in this paper refer only to the nonrelativistic case.

#### *1. Energies and angles*

The use of merged beams has several benefits, particularly for studying low-energy collisions. The relative or interaction energy $E_{\text{c.m.}}$ in the center of mass system (c.m.) of two particles, taken here to be an electron and an ion, in collinear beams is given by

$$E_{\text{c.m.}} = \mu \left[ \left( \frac{E_e}{m_e} \right)^{1/2} - \left( \frac{E_i}{m_i} \right)^{1/2} \right]^2 , \tag{1}$$

where $E_i$, $E_e$, $m_i$, and $m_e$ are the laboratory energies and the masses of the ion and electron, respectively, and $\mu$ is the reduced mass $m_e m_i/(m_e+m_i)$ of the system. Clearly, zero or near-zero $E_{\text{c.m.}}$ can be achieved with various combinations of laboratory energies of the two particles. There is also a "compression" of the relative energy spread of the particles [9] allowing relatively high resolution studies. These features, which are normally thought of as the principal advantages of the merged beams technique and which make the method so effective in recombination studies, are *not* the features emphasized in the technique described here.

Equation (1) shows that both zero energy and other fixed $E_{\text{c.m.}}$ can be obtained using a variety of laboratory energies. This concept provides a very useful diagnostic tool which can be used to probe the differential scattering cross section (DCS) of an electron by an ion as discussed below. Moreover, $E_{\text{c.m.}}$ can be altered significantly by changing the laboratory energy of either beam. In the present experiment, a range of $E_{\text{c.m.}}$ is typically covered using only one laboratory electron energy. For example, for an electron beam with 22.6 eV in the laboratory frame, a c.m. energy range from 13.4 to 10.4 eV can be sampled by tuning the $O^{5+}$ ion beam energy between 35 and 67.5 keV.

An important advantage of the merged-beams approach is the large angular collection of the scattered electrons. Since the beams are traveling in the same direction, scattering angles in the laboratory frame are smaller than the angles in the c.m. frame due to the angular transformation between the c.m. and the laboratory frame which, referring to Fig. 1, is given by

$$\tan\theta_{\text{lab}} = \frac{\sin\theta_{\text{c.m.}}}{\dfrac{V_{\text{c.m.}}}{v_e'} + \cos\theta_{\text{c.m.}}} , \tag{2}$$

where $V_{\text{c.m.}}$ is the velocity of the center of mass, $v_e'$ is the velocity of the scattered electron in the c.m. frame, and $\theta_{\text{c.m.}}$ and $\theta_{\text{lab}}$ are, respectively, the scattering angles of the electron in the c.m. and laboratory frames.

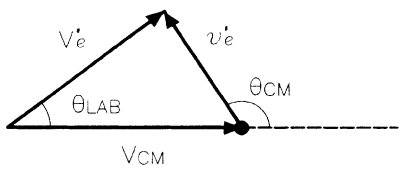


FIG. 1. Vector diagram relating scattering angles $\theta_{\text{c.m.}}$ and $\theta_{\text{lab}}$ in the c.m. and laboratory frames. $V_{\text{c.m.}}$ is the velocity of the center of mass and $v_e'$ and $V_e'$ refer to the postcollisional electron velocities in the c.m. and laboratory frames, respectively.

Electrons that are scattered at more than 90° in the c.m. frame may still be forward scattered in the laboratory frame if $V_{\text{c.m.}}$ is sufficiently large. In our apparatus, electrons scattered at more than 90° in the laboratory frame are lost from the signal detected at the position-sensitive detector (PSD). If the DCS is backward peaked, small changes in the ion velocity (which is basically the center of mass velocity) can lead to large changes in the number of electrons being scattered forward or backward in the laboratory frame. By observing the apparent cross section for a range of ion velocities, rough features of the DCS can be inferred.

### 2. Cross sections

For particles of number densities $N_e$ and $N_i$ colliding with relative velocity $v_r$ and producing collision events at a rate $dS$ in the elemental volume $dV$, the collision cross section for the process is defined through the relation [9,12]

$$\frac{dS}{dV}=N_eN_iv_r\sigma \ . \tag{3}$$

For merged beams traveling in the $z$ direction, the relative velocity can be taken as constant throughout the collision volume. The particle flux $\Gamma_j$ can be written in terms of the number density $N_j$ and particle laboratory velocity $v_j$ by $\Gamma_j=N_jv_j$, and the fluxes are related to the particle electric currents $I_j$ through $I_j=qe\int\Gamma_j(x,y,z)dx\,dy$, where $qe$ is the charge of the particles. Thus, integrating Eq. (3) over the volume of interaction and relating the fluxes to the measured beam density distributions $G(x,y,z)$ and $H(x,y,z)$ measured in arbitrary units yields

$$\sigma=S\frac{v_ev_i}{v_r}\frac{qe^2}{I_eI_i}\left[\frac{\int G(x,y,z)dx\,dy\int H(x,y,z)dx\,dy}{\int G(x,y,z)H(x,y,z)dx\,dy\,dz}\right] . \tag{4}$$

Finally, denoting the term in square brackets by $F$, the form factor, writing $S$ in terms of the *observed* signal $R$ and the detection efficiency $\epsilon$, and noting that for merged beams the relative velocity in terms of the particle laboratory velocities is $v_r=|v_e-v_i|$ we obtain

$$\sigma(E)=\frac{R}{\epsilon}\frac{qe^2}{I_eI_i}\left[\frac{v_ev_i}{|v_e-v_i|}\right]F \ , \tag{5}$$

which is the working relationship for obtaining the cross section from measurables in a merged beams experiment.

## B. Apparatus and technique

### 1. Overview

Figure 2 is a schematic illustration of the merged-beams electron-energy-loss apparatus. The apparatus is

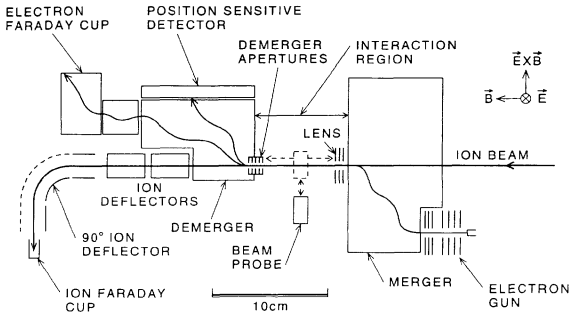


FIG. 2. Schematic view of the merged-beams apparatus.

immersed in a uniform solenoidal magnetic field [13], which has a typical value of 30 G and is parallel to the incident ion beam. Electrons from an electron gun are focused into a region (the merger) having a transverse electric field of about 10 V/mm. The top and bottom plates between which the field is established are biased positive and negative with respect to the plane in which the electron beam enters the merger. We refer to this plane as the "median" plane. In the crossed $E$ and $B$ fields of the merger, the electrons execute trochoidal motion which can be viewed as cyclotron motion about the $B$ field at frequency $\omega_c=eB/m$ and drift perpendicular to the two fields with velocity $\rho=\mathbf{E}\times\mathbf{B}/B^2$. Thus, after an integral number $n$ of cyclotron periods $T_c$, the initial velocity of the electrons is reproduced at the exit of the merger, but the particles are displaced perpendicular to the two field directions by an amount $(E/B)nT_c$. In our case, $n$ is always 2. Multiply charged ions from an electron cyclotron resonance (ECR) ion source [14] are merged with the electrons at the merger exit. Ions and electrons then travel together in an electric-field-free region (about 63.5 mm long) where the collisions take place.

At the end of this collision region, the primary electrons and forward-traveling inelastically scattered electrons are separated by the action of a second pair of parallel plates (the demerger) with an electric field of about 2.5 V/mm. As in the case of the merger, the demerger plates are biased positive and negative with respect to the median plane. The demerger acts as an electron velocity-dispersion device. Unscattered electrons, deflected by the demerger through a relatively small angle, are collected by a Faraday cup and their current is measured. Scattered electrons, deflected through much larger angles, strike a PSD oriented with its plane normal to the $\mathbf{E}\times\mathbf{B}$ direction and are counted. Ions are deflected and collected in a Faraday cup and their current is measured. The operating pressure is approximately $1.5\times10^{-8}$ Pa. The measurement of the extent of electron and ion beam overlap (form factor) along the merge path is accomplished using a movable beam probe [15] employing fluorescent screen and digitized video techniques.

Table I shows typical operating parameters which will be referred to as the experiment is described in more detail.

TABLE I. Typical operating parameters for the $O^{5+}(2s \rightarrow 2p)$ experiment.

| Parameter | Value |
|---|---|
| Laboratory electron energy | 18.7–27.1 eV |
| c.m. electron energy | 10.4–13.6 eV |
| Ion energy | 35.0–67.5 keV |
| Electron current | 200 nA |
| Ion current | 50 nA |
| Form factor | $2.5\times10^{-3}$ cm |
| Signal rate | $<50$ s$^{-1}$ |
| Corrected count rates | |
| {1} Both beams on | 15 100 s$^{-1}$ |
| dead-time correction | 8.4% |
| {2} Electron beam on | 6900 s$^{-1}$ |
| dead-time correction | 3.3% |
| {3} Ion beam on | 8200 s$^{-1}$ |
| dead-time correction | 5.3% |
| {4} Both beams off | 50 s$^{-1}$ |
| dead-time correction | 0.05% |

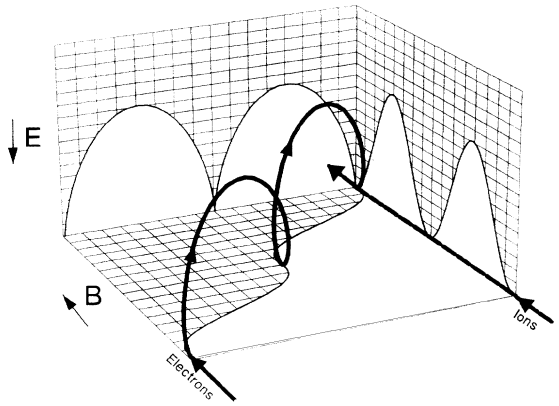


FIG. 3. Demonstration of trajectories of electrons undergoing trochoidal motion in the crossed electric and magnetic fields of the merger. The fields are chosen so that the two beams that are initially horizontally displaced from each other will be on collinear trajectories upon exiting the region of transverse field.

### 2. *Trochoidal motion*

An electron of mass $m$ and charge $e$ in crossed electric and magnetic fields undergoes trochoidal motion as described in many books [16]. Stamatović and Schulz [17] first made use of this motion to make a monoenergetic electron beam. The concept was first implemented to merge and demerge an electron and ion beam by Auerbach *et al.* [11]. Assuming that the particle initially is traveling in the $z$ direction with velocity $\mathbf{v}=\dot{z}_0\mathbf{k}$, that the magnetic and electric fields can be described as $\mathbf{B}=B\mathbf{k}$ and $\mathbf{E}=E\mathbf{j}$, and that the motion starts at the origin, we have

$$\begin{aligned} x &= \frac{\rho}{\omega_c}[\omega_c t-\sin(\omega_c t)] , \\ z &= \dot{z}_0 t , \\ y &= \frac{\rho}{\omega_c}[1-\cos(\omega_c t)] \end{aligned} \tag{6}$$

and

$$\dot{x}=\rho[1-\cos(\omega_c t)],\quad \dot{z}=\dot{z}_0,\quad \dot{y}=\rho\sin(\omega_c t) . \tag{7}$$

Trochoidal motion described by Eqs. (6) and (7) is illustrated in Fig. 3. An important property is that for $t=nT_c=n(2\pi/\omega_c)$ $(n=1,2,3,\ldots)$ the velocity is equal to the *initial* velocity, the coordinate $y$ has its initial value, and $x$ and $z$ are advanced by $\rho nT_c$ and $v_0 nT_c$, respectively. Figure 2 illustrates how these properties are implemented in the current experiment. For a merger of length $L$, an initial displacement between electron and ion beams of $D$, an electron energy of $eV_0$, and choosing $n=2$, one has the defined parameters

$$\begin{aligned} E &= \frac{8\pi V_0 D}{L^2} , \\ B &= \frac{4\pi}{L}\left[\frac{2mV_0}{e}\right]^{1/2} , \\ \rho &= \frac{E}{B}=\left[\frac{2eV_0}{m}\right]^{1/2}\frac{D}{L}=\dot{z}_0\frac{D}{L} . \end{aligned} \tag{8}$$

These equations apply only to electrons with initial velocities parallel to the $z$ axis and in the median plane. In fact complications arise for a finite sized beam, as discussed below.

### 3. *Electron beam*

In the electron gun, electrons emitted from a dispenser cathode are accelerated and focused to produce an electron beam [18] parallel to the ion beam, but displaced horizontally by 64 mm. Under typical conditions for the present experiment, the electron beam current is 200 nA and the beam diameter is approximately 1 mm. Electron laboratory energies for this experiment ranged from 18.7 to 27.1 eV. After formation, the beam enters the merger. The median plane of the merger is set at a few volts (typically about 4 V) below ground potential and thus the electrons have lower energies while in the merger. It was found empirically that the electron beam exited the merger with better spatial characteristics under these conditions.

In practice, the electron beam entering the trochoidal plates has a finite diameter, so that some electrons enter the device above and some below the median plane. Hence some beam electrons are accelerated and some decelerated upon entering, and they thus are not in the merger an integral number of cyclotron periods. Upon exiting, then, a "beam shear" [7,19] has occurred, turning a beam of circular cross section into one which appears as a tilted and elongated ellipse. More problematic is the fact that those electrons exiting high or low have velocity components transverse to the $z$ (merge) axis. The electron distribution $H(x,y,z)$ along the merge path thus exhibits oscillations and "scalloping," and its careful measurement all along the merge path is essential. Electrostatic lenses before and after the merger help correct for distortions of the beam due to the beam shear. Beam shear effects on the primary merging electron beam can be kept to a minimum by using a very small diameter

electron beam injected into the merger [20]. However, the secondary "beams" of electrons resulting from inelastically or elastically scattered primary electrons have a relatively large effective diameter due to angular scattering, and beam shear effects in the demerger substantially reduce the effective dispersive quality of the demerger.

As discussed above, upon exiting the merger the velocity and shape of the original electron beam is approximately maintained, except that the electrons are now merged with the ions and travel with the ions through an electric field free region is that is about 63.5 mm long. To minimize beam shear effects, careful "tuning" of the electron beam is imperative or background count rates at the PSD due to electrons scattering off surfaces become prohibitively large. Though moving radially and scalloping slightly along the merge path, the electrons are generally contained within an imaginary tube along the ion beam with a diameter of 1.5 mm.

In the demerger the primary electron beam is deflected through about 17° and collected in a specially designed Faraday cup, the final element of which is a pair of plates producing further trochoidal motion. The primary beam contains about $10^{12}$ electrons $s^{-1}$, while the signals sought are only a few tens of counts per second; so it is imperative to have *no* electrons returning from the Faraday cup to the PSD.

#### 4. Ion beam

The multiply charged $O^{5+}$ ions are extracted from the ECR ion source [14] and are accelerated to the desired energy, ranging from 35 to 67.5 keV for the present experiment, mass analyzed, collimated, passed through several stages of differential pumping, and then directed into the experimental chamber. A typical $O^{5+}$ beam in the experimental apparatus has a current of 50 nA (electrical) and a diameter of 1.5 mm. The ions travel through the electric field of the merger before entering the interaction region and through the field of the demerger upon exiting. However, since $\omega_c^i \ll \omega_c^e$, Eq. (6) shows that these fields do not affect the ion beam to a significant extent, and deflectors before the merger and after the demerger adequately compensate for the small deflections incurred.

After passing through the demerger, the ions are deflected by 90° and are collected in a suppressed Faraday cup from which their current is measured. Deflection of the ion beam before collection ensures that secondary electrons produced at the ion Faraday cup do not travel back to the PSD and makes it easier to shield the PSD from photons produced by ions hitting their collector.

#### 5. Beam probe

The form factor $F$ given by the square brackets in Eq. (4) is measured using a fluorescent-screen digitized-video technique which we have described previously [15]. The probe is capable of measuring the two-dimensional beam intensity distributions at arbitrary intervals along the beams' paths. Given the distributions, the "beam overlap" $\Omega$ is computed at each $z$ for which a measurement is made, where

$$\Omega(z)=\frac{\int G(x,y,z)H(x,y,z)dx\,dy}{\int G(x,y,z)dx\,dy \int H(x,y,z)dx\,dy} \tag{9}$$

and $G(x,y,z)$ and $H(x,y,z)$ are the two-dimensional ion and electron beam density distributions, measured at the several positions. The integral of $\Omega(z)$ is then performed to get the form factor $F$.

With the probe one can take two-dimensional current distributions of either beam at arbitrary positions along approximately 45 mm of the 63.5-mm total merge path. The remaining portion of the merge path is inaccessible to the probe motion and the overlaps for these regions must be extrapolated. The value of the overlaps in these regions is taken to be the average value over the measured path. Typically, pictures are taken at seven positions in the interaction region. Taking pictures at more positions does not measurably increase the precision of the measurement and it significantly increases the time involved taking overlaps and calculating the form factor.

The probe is constructed to enable the real-time observation of either the electron or ion beam as well as to enable digitized current distributions to be measured, and one can thus observe the shape and location of either beam on an oscilloscope while tuning the beams for desired characteristics.

#### 6. Detection of inelastically scattered electrons

This experiment is designed to detect those electrons which have lost energy by exciting the ion target. Electrons which have lost energy in a collision and are scattered at less than 90° in the laboratory frame [see Eq. (2)] enter the demerger with forward velocities less than the primary electron beam. Hence they travel in the demerger at an angle with respect to the $z$ direction given approximately by $\tan\theta=\rho/v_f$, where $v_f$ is the forward velocity of the entering electron. After traveling the width of the demerger, the electrons strike the PSD and are counted. Electrons backscattered in the laboratory frame do not enter the demerger and are not detected.

The PSD is located at the edge of the demerger parallel to the $z$ axis. The detector is assembled from two commercial microchannel plates [21] and a resistive anode [22] and is fronted by a transparent (94%) grid and a series of 0.03-mm wires attached to a voltage divider to maintain the uniform field up to the edge of the demerger. Pulses from the four corners of the resistive anode are amplified, fed into a position computer [23], and decoded to determine the position of the event on the PSD. The event is then assigned to one of $64\times256$ pixels of the PSD and gated into one of four temporally distinguished (see below) recording channels.

Low-energy inelastically scattered electrons that enter the demerger below the median plane can be reflected from the demerger due to the negative potential encountered. A scattered electron from a threshold excitation of a 50-keV $O^{5+}$ ion will have a kinetic energy of 1.69 eV in the laboratory frame and will be rejected if it enters the demerger 0.85 mm below the median plane. Therefore,

to ensure that signal electrons are not being rejected, the median plane of the demerger is biased at 1.5 V above the potential of the collision region so that electrons are accelerated into the demerger. This acceleration reduces the dispersion of the demerger, but collection of signal electrons is of paramount importance. The beam overlaps as a function of $z$ were used to determine the distribution of positions at which inelastically scattered electrons were produced. This information was used in a "demerge program" incorporating the SIMION trajectory computer program [24] to determine the extent to which all electrons were collected and thus to give guidance when parameters should be adjusted to ensure collection.

Modeling of the inelastically scattered electrons in the demerger region has also been carried out using the MAFIA computer code [25]. MAFIA allows a full three-dimensional description of electrodes and trajectories. Two-dimensional codes such as SIMION are inaccurate for the mixed geometries (planar and cylindrical) that are present in the demerger and demerger apertures. MAFIA was used to simulate the electrode geometry as well as the electron trajectories in the demerger apertures and demerger. The model predicted that inelastically scattered electrons should start to be lost at about 1.7 eV above threshold and predicted accurately the observed location of signal on the PSD. It was, however, too tedious to use this code on a routine basis, and it therefore was used primarily to verify the modeling results using SIMION and visual judgment of the signal location on the PSD.

If inelastically scattered electrons are scattered into the backward direction in the c.m. frame, then as seen in Fig. 1 and Eq. (2), when $v_e'\cos\theta_{\text{c.m.}} > V_{\text{c.m.}}$ the scattering will be in the backward direction in the laboratory frame as well and the electrons will not enter the demerger. Clearly, by varying $V_{\text{c.m.}}$ one can investigate the gross character of the differential cross section for the inelastic collision under investigation. For the present experiment, the upper limit to $V_{\text{c.m.}}$ was set by limits on the voltage which could be applied to the 90° ion deflector after the demerger.

The detection efficiency is measured by directing a strongly attenuated beam of electrons (1–5 fA) alternately into a Faraday cup, where the current was measured with a vibrating reed electrometer and then onto the PSD where the particles were counted. The measured detection efficiency is $0.70\pm0.02$, a value orders of magnitude larger than efficiencies for crossed beams fluorescence experiments. By directing current to different parts of the PSD, the efficiency was observed not to vary significantly over the active area normally used.

### 7. *Data acquisition*

The data acquisition scheme is shown in Fig. 4. The experiment is controlled by a computer [26] and a CAMAC crate via an IEEE-488 data bus. Signal pulses with position information are routed from the PSD through the position computer to one of four histogramming memories, depending on which of the beams are on at the time. Beam modulation and signal count gating

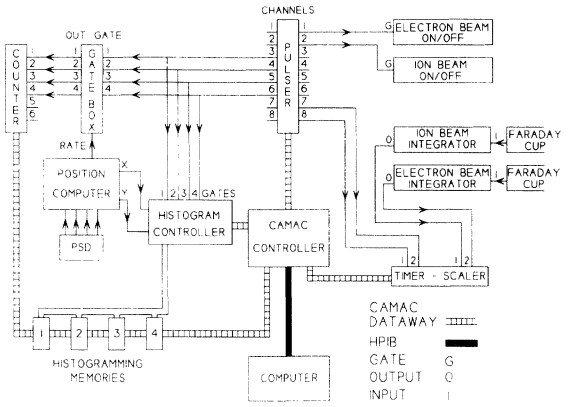


FIG. 4. Schematic diagram of the data acquisition system. PSD denotes a position-sensitive detector.

are controlled by the pulser—a homebuilt unit—that supplies fast TTL logic level wave forms with adjustable durations. The counts from the rate output (pulses unprocessed to determine position) of the position computer are collected in four channels of a fast counter. Electron and ion primary beam currents and "on" times are measured using the current integrators and timers.

Although the pressure in the vacuum chamber is maintained at $1.5\times10^{-8}$ Pa under experimental conditions, the ratio of signal electrons to background events is low. Under typical experimental conditions, the PSD receives approximately 80 Hz of signal electrons, but also records about 15 kHz of counts due to electrons and ions colliding with background gas and surfaces. The background due to the electrons is about 50 Hz/nA, while that due to the ions is about 100 Hz/nA.

To make it possible to extract the signal from the background, both beams are modulated at 1000 Hz in a phased four-way chopping scheme [7] as shown schematically in Fig. 5. The logic for this chopping is supplied by the pulser. Adjustable delays (normally set to 25 $\mu$s) are used between the times the beams switch off or on and

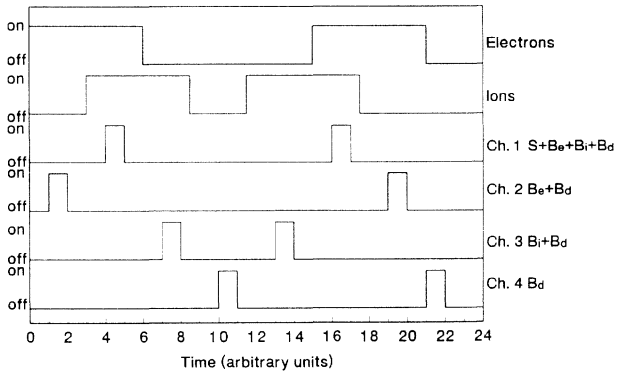


FIG. 5. Wave-form sequence of the pulser used to modulate electron and ion beams and to gate the four histogramming memories.

the beginning of data collection to allow the beams ample time to stabilize. The alternating phases are included to obviate errors associated with one beam's systematically switching on before the other. Thus, in the first phase (near time element 5) the signal is collected after the electrons have been on for a half cycle and the ions have just been switched on. In the second phase (near time element 17) the signal is collected after the electrons have just been switched on and the ions have been on for a half cycle. Modulation of the beams at less than about 200 Hz showed some slight evidence of spurious signal due to pressure modulation effects, so the chopping frequency was chosen to be 1000 Hz. Phased four-way modulation of both beams at 1000 Hz and using 25 $\mu$s settling times corresponds to a duty factor of only about 15% for data taking in the signal channel.

As already discussed and shown in Figs. 4 and 5, data are collected in four different channels, corresponding to different beams' being on during the various phases of the chopping sequence. If we define $R$, $B_e$, $B_i$, and $B_d$ as the signal, background due to the electron beam, background due to the ion beam, and dark count rates, respectively, then the four channels as shown in Fig. 4 record $\{1\}$ both beams on (collecting $R+B_e+B_i+B_d$), $\{2\}$ ion beam off and electron beam on (collecting $B_e+B_d$), $\{3\}$ ion beam on electron beam off (collecting $B_i+B_d$), and $\{4\}$ both beams off (collecting $B_d$). The signal is determined by performing the operation

$$R=\{1\}-\{2\}-\{3\}+\{4\}\ , \tag{10}$$

but *only* after correcting the count rates for each channel for dead times of the system as discussed later. Typical values of corrected count rates are shown in Table I.

The typical procedure for taking a data point begins by choosing a suitable combination of laboratory electron energy and ion energy that gives the desired collision energy and to fine-tune the beams to minimize the backgrounds and optimize the overlaps. Next, the form factor is measured and data accumulation is begun. The data taking is divided up into cycles. For each cycle, count rates from the detector are accumulated and beam currents are measured for about 60 s, the results are read and analyzed [dead-time corrections, and cross sections calculated via Eq. (5)] by computer, running totals are stored, the registers are reset, and the next data taking cycle is initiated. Typically, each cross section data point at a fixed collision energy takes about 1.5 h to reach the desired statistical precision. Cumulative histograms $\{1\}$, $\{2\}$, $\{3\}$, $\{4\}$, and $\{R\}$ are available at the end of this time for further analysis. The collision energy is then altered, often by changing the ion energy, and the data accumulation process is restarted.

Signal events from inelastically scattered electrons typically are located on select areas of the PSD, whereas background events are more broadly distributed. Using software, the signal area can be delimited using both modeling and visual selection. This significantly cuts down statistical uncertainties due to background, but does not affect the signal.

### 8. *Dead-time corrections*

The issue of dead-time corrections to the data is one of the most subtle and difficult parts of the experiment. There are three different dead times involved: $\tau_p$, the dead time of the microchannel plate and anode; $\tau_r$, the dead time of the rate (all entering pulses) channel of the position computer; and $\tau_s$, the dead time of the strobe (position-analyzed events) channel of the position computer. The first of these can be calculated by methods suggested by Wiza [27] to be about 20 ms per microchannel, or about 0.22 ms per pixel of the position computer. We have measured the value to be 0.21 ms per pixel in good agreement with the calculation. Because of the spread-out nature of the signal in terms of pixels, it is seldom that this correction is significant, but nevertheless, the correction is made pixel by pixel. The dead time of the rate channel is suggested by the manufacturer to about 0.6 $\mu$s and measured by us to be $0.65\pm0.1$ $\mu$s, and the strobe dead time is suggested by the manufacturer to be about 3 $\mu$s and measured by us to be $3.58\pm0.02$ $\mu$s (see the Appendix for a discussion of paralyzable and nonparalyzable dead times).

Each of the four histogram distributions is dead-time corrected at the end of each cycle. It is *absolutely essential* that these memories be separately corrected, even when the corrections are small, since the signals sought after are also very small compared to the backgrounds. An example using typical values illustrates this. Assume one has 200 nA of 24.1-eV electrons colliding with 50 nA of 55-keV $O^{5+}$ ions with an overlap of $2.5\times10^{-3}$ cm, cross section of $2.5\times10^{-16}$ cm$^2$, and detection efficiency of 0.7. Then by Eq. (5), we expect the signal rate $R$ to be 49 s$^{-1}$. Suppose further that the background on the PSD due to presence of electrons is $10^4$ s$^{-1}$, that due to ions is 5000 s$^{-1}$, and to other background sources 100 s$^{-1}$. In the rate channel, one would measure the values of 15 001, 10 034, 5083, and 100, respectively, for $\{1\}$, $\{2\}$, $\{3\}$, and $\{4\}$ and the apparent signal of $R=-16$. In the strobe channel one would measure the respective values of 14 349, 9741, 5008, and 100 and the apparent signal of $R=-300$. There is clearly no way to simply combine these numbers before individually correcting them for dead time. The correction is accomplished using a rapidly converging iterative procedure for solving the transcendental equation [Appendix, Eq. (A1)], starting with using the observed count rate in place of the unknown input count rate. The strobe channel dead time must be very accurately determined since the signals are such a small fraction of the total counts.

### 9. *Elastically scattered electrons and other unwanted signals*

In the discussion to this point, it has been assumed that inelastically scattered electrons are the only source of signal counts which will result in a finite value of $R$ in Eq. (10). In fact, there are several possible sources which must be eliminated or accounted for. The existence of such sources generally becomes evident from the presence of signal at electron energies below the excitation threshold.

Foremost of these possible sources of spurious signal is

elastic scattering of electrons by the ions. Electrons may elastically scatter from an ion into some angle which results in *forward* velocities (components in the $+z$ direction) which are identical to those of inelastically scattered electrons. Since the demerger acts to disperse only forward velocities, these electrons will strike the PSD in the same area as those inelastically scattered. Of course, these electrons occur in exactly the correct temporal pattern to register as signal as well. The cross sections for elastic scattering are very large and increase as the square of the target charge; thus this spurious signal is much worse for multiply charged ions.

In order to keep these elastically scattered electrons from reaching the detector, a series of five apertures (each 5 mm in diameter) is installed at the entrance to the demerger. Electrons scattered at a large enough angle that their *forward velocities* would enable them to reach the PSD have *radial* velocities large enough that their cyclotron radii are so large that they cannot pass the apertures. The series of five apertures ensures that all phases of the cycloidal trajectories are stopped. However, this still leaves some elastically scattered electrons in the "throat" of the apertures and at the entrance to the demerger. In order to mitigate this problem, the beams are "tuned" so that there is good overlap in the "upstream" portion of the interaction region and poor overlap in the "downstream" portion and most particularly at the end of the merge path. This procedure prevents electrons from elastically scattering off ions where the product electrons could reach the PSD. A typical series of measured overlaps as a function of $z$ is shown in Fig. 6, demonstrating the near-zero overlap at $z=-30$ mm where the entrance to the demerger lies.

A spurious signal, which has already been alluded to earlier, arises when either beam causes the pressure in the vicinity of the beams to be modulated and the beams then scatter off a gas whose density is changing in a phased way to give an apparent signal. The approximately 300 l volume and 1000 $1\,s^{-1}$ pumping speed give a time constant for the vacuum system of about 0.3 s. Spurious effects from this source are diminished [9,12] by the ratio of this time constant to the chopping time period and are further reduced by a phase shift. Of course, more local regions of the apparatus can have shorter time constants and there is also the possibility of "beaming" effects from desorbed gases (e.g., from the Faraday cup). As was already mentioned, systematic tests to observe such spurious signals indicated that chopping at frequencies above 200 Hz ensured the absence of these problems and operating normally at 1000 Hz provides a comfortable margin.

Other spurious signals may result when the space charge of one beam modulates the background from the other beam. This is particularly a problem when the beams-caused backgrounds originate from the beams hitting surfaces and is best avoided by proper tuning of the beams to minimize such backgrounds. One instance was found of the ion beam directly modulating the electron background when the einzel lens at the exit of the merger was operated at a negative potential in order to minimize shear effects and radial velocities of the electrons in the collision region. This mode was subsequently avoided. Regular tests indicate that it is possible generally to avoid the space-charge modulation source of spurious signals.

## III. RESULTS FOR $O^{5+}$

### A. Total cross section

The total measured absolute excitation cross sections for electron-impact excitation of $O^{5+}$ $(2s \rightarrow 2p)$ versus interaction energy in the c.m. system are shown as the solid points in Fig. 7 and listed in Table II. Most points are the weighted average of several data runs. Error bars represent an expanded uncertainty [28] $U_r$ defining a lev-

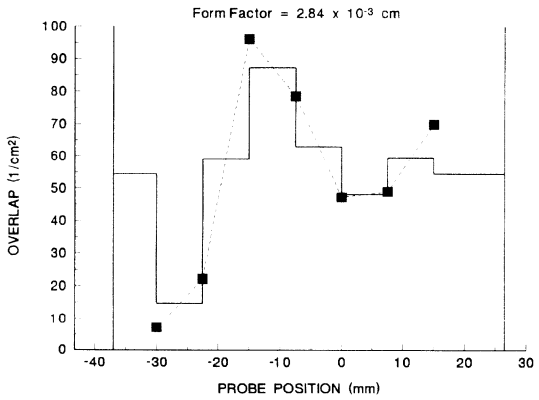


FIG. 6. Example of a measured form factor showing beam overlaps $\Omega$ vs probe position. Solid points represent measured overlaps. The two vertical lines show the extent of the merge path: the electron beam is merged with the ion beam at approximately $+27$ mm and is demerged at $-37$ mm. The solid horizontal lines represent deduced average overlap values in the respective intervals which are then used for the numerical integration of $\Omega$ along $z$ to get $F$.

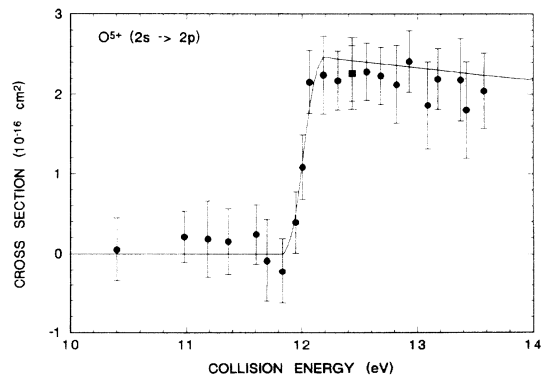


FIG. 7. Total absolute electron-impact excitation cross sections for $O^{5+}(2s \rightarrow 2p)$ versus collision energy in eV. Error bars represent an expanded uncertainty $U_r$ where a coverage factor of $k=2.0$ has been used to set an approximate confidence interval of 90% for relative uncertainties. The outer bar at 12.4 eV represents the total uncertainty (quadrature combination of relative and systematic uncertainties) at a similar confidence level.

TABLE II. Excitation cross-section results for $O^{5+}(2s \rightarrow 2p)$. Expanded relative uncertainties $U_r$ are listed, where a coverage factor of $k=2.0$ has been used to set an approximate confidence level on $U_r$ of 90%. Total systematic uncertainties are estimated to be ±6% with a similar confidence interval.

| Energy (eV) | $\sigma \pm \Delta\sigma$ ($10^{-16}$ cm$^2$) | Energy (eV) | $\sigma \pm \Delta\sigma$ ($10^{-16}$ cm$^2$) |
|---|---|---|---|
| 10.40 | 0.05±0.39 | 12.31 | 2.17±0.37 |
| 10.98 | 0.21±0.32 | 12.43 | 2.26±0.35 |
| 11.18 | 0.18±0.47 | 12.56 | 2.28±0.36 |
| 11.36 | 0.15±0.41 | 12.69 | 2.23±0.36 |
| 11.61 | 0.24±0.37 | 12.82 | 2.12±0.49 |
| 11.70 | −0.09±0.52 | 12.93 | 2.41±0.38 |
| 11.83 | −0.22±0.41 | 13.09 | 1.86±0.55 |
| 11.95 | 0.39±0.38 | 13.18 | 2.19±0.38 |
| 12.01 | 1.08±0.41 | 13.38 | 2.18±0.52 |
| 12.06 | 2.15±0.39 | 13.43 | 1.80±0.61 |
| 12.18 | 2.24±0.49 | 13.58 | 2.04±0.47 |

el of confidence of about 90% (a coverage factor $k=2.0$ was used) for relative uncertainties. Relative uncertainties are those which may affect the shape of the curve as well as the value and they are determined by a quadrature sum of contributions from uncertainties resulting from counting statistics, form factor fluctuations, and determining the area occupied by the signal on the PSD. The measurements extend from 1.6 eV below the excitation threshold of 12.01 up through 1.6 eV above the threshold. The outer error bar on the point at 12.4 eV signifies the total uncertainty $U_t$, which is the quadrature combination of $U_r$ and systematic uncertainties composed of uncertainty in the detector efficiency, uncertainties in the electron and ion current measurements, uncertainties due to dead-time corrections, and absolute uncertainty in the form factor. The latter are estimated to be at a similar confidence interval as $U_r$.

The solid curve in Fig. 7 represents a seven state close-coupling calculation of Griffin, Badnell, and Pindzola [29] that has been convoluted with the 0.20-eV energy spread found for our electron beam. The agreement between the theoretical calculation and the experimental data is seen to be very good. Results near threshold from a two-state close-coupling calculation of Robb [30] lie about 2% above those of Ref. [29], while results from a distorted-wave calculation of Davis [30] lie about 15% higher.

The energy spread of the electron beam was determined by observing the threshold of the excitation. Convoluting the step at the onset of excitation with a Gaussian distribution and fitting the resulting curve to the data yielded an energy spread for this experiment of 0.20-eV full width at half maximum. This energy spread is consistent with that observed in earlier experiments [5,6] performed with this apparatus.

### B. Correction for target impurity

Measurements at interaction energies below the excitation threshold yielded nonzero signals which were strongly correlated with ion energy. The discussion above notes a number of possible sources of spurious signals. In addition, another possible source was hypothesized and modeled. In this model, it was assumed that there were ions in the beam which were in metastable doubly excited states $1s2snl\ ^4J$, which are forbidden to spontaneously autoionize, but which have a very large cross section for ionization during a collision with an incident electron.

Each of these hypothesized sources of spurious signal was modeled, and derived corrections were made according to each model. After the modeled correction for the assumed spurious source, the data were examined for correlation with the experimental parameters, Table III shows the correlation with each of these models both before and after the "correction" and it is observed that the only model which removes the correlation is the model assuming autoionizing contaminants. The data presented in Fig. 7 and Table II have consequently been corrected for this effect.

Fitting the below-threshold raw data versus the ion transit time to the experimental chamber yields an effective lifetime of approximately 0.9 $\mu$s. The lifetime of the $1s2s2p\ ^4P$ state has been calculated to be 40 ns [31], a value much shorter than that observed. However, one may hypothesize [32] that high-lying Rydberg quartet states may have such a long lifetime, since high Rydberg states would not readily interact with the $2s$ electron and cascade to lower levels could easily be on the order of a microsecond. Using the method of Welton, Morgan, and Thomas [33], it is possible to determine that the expected population of the $1s2s2p\ ^4P$ state in the primary beam to be on the order of 1%. If it is assumed that the population of all quartet states in the beam is of this order, and if the further assumption is made that a "destroyed" autoionizing state results in a count on the detector, then

TABLE III. Correlation coefficients of below-threshold cross-section data with experimental variables.

| Data | Ion energy | Electron energy (laboratory) | Electron energy (c.m.) | Ion background |
|---|---|---|---|---|
| Raw data | 0.80 | 0.65 | −0.18 | 0.57 |
| Data after modeled correction for | | | | |
| modulation effects | 0.80 | 0.68 | −0.13 | 0.56 |
| elastic scattering | 0.80 | 0.73 | −0.02 | 0.55 |
| 0.9-$\mu$s metastable states | 0.09 | 0.03 | −0.06 | 0.02 |

one can estimate on the basis of the below-threshold data that the cross section for destruction of the autoionizing state by collision with an electron is greater than $\sim 10^{-14}$ cm$^2$.

When the lowest ion energy (35 keV) was used so that the autoionizing metastables had maximum opportunity to decay in flight in the collision region, the corrections to the measured cross sections were about $0.3\times10^{-16}$ cm$^2$. In contrast, when the maximum ion energy of 67.5 keV was used, the corrections were about $1.1\times10^{-16}$ cm$^2$. It is emphasized, as Table III shows, that after the corrections, the data taken with different ion energies agree.

### C. Backscattering

As noted earlier, small changes in the velocity of the center of mass can lead to large changes in the number of electrons forward or backward scattered in the laboratory frame, particularly if the ion has a backward peaked DCS. Since the merged beams apparatus only collects electrons that are scattered in the forward direction in the laboratory frame, backscattering will manifest itself as a reduction in the apparent cross section $\sigma_{app}$ observed at the PSD as the ion velocity is decreased. The rough features of the DCS can be determined by observing $\sigma_{app}$ versus the velocity of the center of mass.

Under experimental conditions, backscattering was observed by measuring data points for a constant laboratory electron energy, successively changing the ion energy and observing $\sigma_{app}$. An example of such a set of measurements can be seen in Fig. 8. Here the electron laboratory energy was fixed at 24.1 eV and the ion energy was scanned from 39 to 54.7 keV with a corresponding range of velocities of $(6.81-8.07)\times10^5$ m/s. For this range of ion energies the postcollisional electron velocities varied from $(8.60-4.44)\times10^5$ m/s. These combinations of velocities clearly allow for the observation of backscattering. The experimental data are shown with error bars representing expanded relative uncertainties at 90% confidence level (coverage factor of $k=2.0$). The solid curve shows the result of a computer program that simulates electron trajectories (ignoring the fringe field of the demerger) with an initial energy corresponding to the experimental energy and using the theoretical DCS to determine which electrons will reach the PSD and be counted as signal. The agreement between this simple model and the experiment is good. If one assumes a forward scattered distribution [34] (illustrated by the short-dashed curve) or an isotropic distribution (shown by the long-dashed curve), the agreement is not good.

Backscattering has been confirmed using quantum-mechanical calculations. The distorted wave DCS result versus c.m. scattering angle [35] is shown as the dashed curve in the inset of Fig. 8. A close-coupling calculation [29] (illustrated as the solid curve of the inset) predicts an almost identical angular distribution. The calculations predict that over 90% of the incident electrons will be scattered at greater than 90° in the c.m. frame. Both calculations shown are for 13.0-eV collision energy, and the calculations indicate no significant change of the DCS over the range of collision energies investigated here.

A semiclassical approach to the calculation also shows a backscattering effect. The principle for this calculation is to follow the trajectories of electrons classically except at closest approach to the ion, where the electron loses 12.01 eV suddenly. Imposing the further constraint (Huber *et al.* [36]) of requiring the transfer of one unit of angular momentum, the scattering angle can be determined. The scattering angle calculated using this method yields 106° and is shown by the arrow in the inset of Fig. 8. This angle is very close to the position for the max-

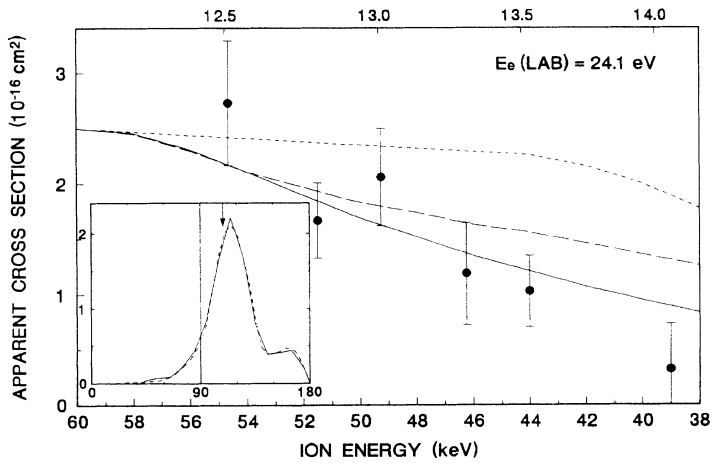


FIG. 8. Points are measured apparent cross section $\sigma_{app}$ versus ion energy (bottom scale) or collision energy (top scale) for a fixed laboratory electron energy of 24.1 eV. Error bars represent an expanded uncertainty giving 90% confidence level for relative uncertainties. Curves correspond to modeled $\sigma_{app}$ using theoretical DCS which are as follows: ——, backward peaked (Ref. [29]); — —, isotropic; and — — —, forward peaked (Ref. [34]). Inset gives theoretical DCS vs collision energy from close-coupling (Ref. [29]) (solid curve) and distorted-wave (Ref. [35]) (dashed curve) methods. The arrow at 105° in the inset represents the result of the semiclassical calculation for the scattering angle.

imum DCS from the quantum-mechanical calculations.

As already discussed, the backscattering limits the collision energy to 1.6 eV above threshold. At collision energies below this limit, the results are not affected.

## IV. CONCLUSIONS

The merged-beams electron-energy-loss technique described here presents an attractive alternative to the traditional crossed-beams fluorescence-detection technique by which absolute cross sections can be measured for electron-impact excitation of multiply charged ions. The detection sensitivity of order unity, compared to typically $10^{-4}$ for the fluorescence approach, is the major advantage, though preempting the need for absolute radiometry is also an important factor. A further benefit is that gross features of the DCS can be extracted from measurements. The chief drawback of a rather narrow energy range above threshold, however, is an important limitation of the technique. The method complements the recently introduced trapped ion techniques which are valuable for very highly charged ions.

Results are reported here for absolute total electron-impact excitation cross sections for the $O^{5+}(2s \rightarrow 2p)$ transition from below threshold to 1.6 eV above threshold. The experimental data are in good agreement with a seven state close-coupling calculation throughout the energy range. The data show that the excitation process results in a dominance of backscattering of the electrons, consistent with calculations that indicate more than 90% of the scattered electrons are in the backward direction in the c.m. frame.

Evidence was observed for doubly excited metastable autoionizing states of $O^{5+}$ with a lifetime of about 0.9 $\mu$s which are made to ionize by electron impact with a cross section approaching $10^{-14}$ cm$^2$.

## ACKNOWLEDGMENTS

We are grateful to D. C. Griffin, N. Badnell, and M. S. Pindzola for allowing use of their close-coupling calculations before publication. We thank K. T. Chung for his discussion of the lifetimes of the excited autoionizing states of $O^{5+}$, J. W. Hale for his skilled technical assistance, and the AT-7 code group at Los Alamos National Laboratory for the use of the MAFIA modeling program and for providing assistance with the operation of the program. This work was supported in part by the Office of Fusion Energy of the U.S. Department of Energy under Contract No. DE-A105-86ER53237 with the National Institute of Standards and Technology and Contract No. DE-AC05-84OR21400 with Martin Marietta Energy Systems, Inc. M.E.B. was supported through the DOE Laboratory Cooperative Postgraduate Research Training Program administered by Oak Ridge Associated Universities.

## APPENDIX: DEAD-TIME CORRECTIONS

As noted earlier, correction of the raw data for the effects due to the dead time of the counting system is among the most crucial aspects of this experiment. In correcting the measured count rates to account for the dead time of the system, one must first determine whether the components of the electronics chain are paralyzable or nonparalyzable [37]. The necessary corrections to the data are different depending on the type of component present.

Once a paralyzable element is triggered into its active state, it remains in that state for a time $\tau_p$. If another pulse is received during this interval, the element is reset and the active interval is extended. Thus the component will not output another valid pulse until a time $\tau_p$ has elapsed without an input pulse occurring. An example of this type of element is a pulse pileup rejector. In contrast, a nonparalyzable component, once triggered, is active for a definite time $\tau_n$ before becoming ready to accept another pulse. An example of this type of component is an analog-to-digital converter.

For a paralyzable element with randomly arriving events at a rate of $R_{\text{in}}$, the measured count rate $R_{\text{out}}$ is

$$R_{\text{out}} = R_{\text{in}} e^{-R_{\text{in}}\tau_p} , \tag{A1}$$

where $\tau_p$ is the dead time. In the case of a nonparalyzable element, the expression for $R_{\text{out}}$ becomes

$$R_{\text{out}} = \frac{R_{\text{in}}}{1 + R_{\text{in}}\tau_n} , \tag{A2}$$

where $\tau_n$ is the dead time.

We were informed by the manufacturer of the position computer that the rate channel of the instrument is totally paralyzable and that the strobe channel is a mix of paralyzable and nonparalyzable systems. By using clock pulses fed into the system, we determined that both channels behave as totally paralyzable. Thus, for our position computer and electronics chain, the elements are all wholly paralyzable, so Eq. (A1) is solved by iteration to determine $R_{\text{in}}$.

[1] For reviews see G. H. Dunn, in *The Physics of Ionized Gases,* edited by M. Matic (Boris Kidric Institute, Belgrade, 1980), p. 49; D. H. Crandall, in *Physics of Ion-Ion and Electron-Ion Collisions,* edited by F. Brouillard and J. W. McGowan (Plenum, New York, 1983), p. 201; R. A. Phaneuf, in *Atomic Processes in Electron-Ion and Ion-Ion Collisions,* edited by F. Brouillard (Plenum, New York, 1986), p. 117. For a comprehensive listing and bibliography see Ref. [2].

[2] E. W. Bell, Ph.D. thesis, University of Colorado, 1993, available through University Microfilms International (UMI), P.O. Box 1764, Ann Arbor, MI 48106.

[3] P. O. Taylor, D. C. Gregory, G. H. Dunn, R. A. Phaneuf, and D. H. Crandall, Phys. Rev. Lett. **39**, 1256 (1977); D. C. Gregory, G. H. Dunn, R. A. Phaneuf, and D. H. Crandall, Phys. Rev. A **20**, 410 (1979); D. S. Belić, R. A. Falk, G. H. Dunn, D. C. Gregory, and C. Cisneros, Bull. Am. Phys. Soc. **26**, 1315 (1981).

[4] R. E. Marrs, M. A. Levine, D. A. Knapp, and J. R. Henderson, Phys. Rev. Lett. **66**, 257 (1991).

[5] E. K. Wåhlin, J. S. Thompson, G. H. Dunn, R. A. Phaneuf, D. C. Gregory, and A. C. H. Smith, Phys. Rev. Lett. **66**, 157 (1991); in *Atomic Physics of Highly Charged Ions,* edited by E. Salzborn, P. H. Mokler, and A. Müller (Springer-Verlag, Berlin, 1991), p. 35.

[6] X. Q. Guo, E. W. Bell, J. S. Thompson, G. H. Dunn, M. E. Bannister, R. A. Phaneuf, and A. C. H. Smith, Phys. Rev. A **47**, R9 (1993); in *VIth International Conference on the Physics of Highly Charged Ions,* edited by P. Richard, M. Stockli, C. L. Cocke, and C. D. Lin, AIP Conf. Proc. No. **274** (AIP, New York, 1993), p. 463.

[7] C. A. Timmer, Ph.D. thesis, University of Colorado, 1988, available through UMI, P.O. Box 1764, Ann Arbor, MI 48106, Order No. AAC 8819709; E. K. Wåhlin, Ph.D. thesis, University of Colorado, 1990, available through UMI, Order No. AAC 9117090.

[8] S. J. Smith, A. Chutjian, J. Mitroy, S. S. Tayal, R. J. W. Henry, K. F. Man, R. J. Mawhorter, and I. D. Williams, Phys. Rev. A **48**, 292 (1993); S. J. Smith, K. F. Mann, R. J. Mawhorter, I. D. Williams, and A. Chutjian, Phys. Rev. Lett. **67**, 30 (1991).

[9] G. H. Dunn, in *Atomic Physics,* edited by B. Bederson, V. M. Cohen, and F. M. J. Pichanick (Plenum, New York, 1969), Vol. I, p. 417.

[10] *Recombination of Atomic Ions,* edited by W. G. Graham, W. Fritsch, Y. Hahn, and J. A. Tanis (Plenum, New York, 1992).

[11] D. Auerbach, R. Cacak, R. Caudano, T. D. Gaily, C. J. Keyser, J. W. McGowan, J. B. A. Mitchell, and S. F. J. Wilk, J. Phys. B **10**, 3797 (1977).

[12] G. H. Dunn, in *Electron-Impact Ionization,* edited by T. D. Märk and G. H. Dunn (Springer-Verlag, New York, 1985), p. 277.

[13] The field is uniform to better than $10^{-4}$ over a cylinder 31 cm long by 41 cm in diameter for fields 0.002 T and greater and is uniform to better than $10^{-3}$ at 0.0002 T. The solenoid is wound according to principles described by M. E. Gardner, J. A. Jungerman, P. G. Lichtenstein, and C. G. Patten, Rev. Sci. Instrum. **31**, 929 (1960); and the shields were constructed according to R. J. Hansen and F. M. Pipkin, Rev. Sci. Instrum. **36**, 179 (1965). The field was aligned to within 250 $\mu$rad by externally rotating the solenoid about axes parallel to both the $x$ and $y$ axes while optimizing electron current to a field alignment Faraday cup (not shown).

[14] F. W. Meyer and J. W. Hale, Rev. Sci. Instrum. **61**, 324 (1990).

[15] J. L. Forand, C. A. Timmer, E. K. Wåhlin, B. D. DePaola, G. H. Dunn, D. Swenson, and K. Rinn, Rev. Sci. Instrum. **61**, 3372 (1990).

[16] J. R. Pierce, *Theory and Design of Electron Beams* (Van Nostrand, New York, 1954), p. 26; L. Spitzer, Jr., *Physics of Fully Ionized Gases* (Interscience, New York, 1956), p. 3; L. D. Landau and E. M. Lifshitz, *The Classical Theory of Fields* (Pergamon, Oxford, 1962), p. 62.

[17] A. Stamatović and G. J. Schulz, Rev. Sci. Instrum. **41**, 423 (1970).

[18] The electron gun was designed using modeling with the "E−Gun" program, W. B. Hermannsfeldt, SLAC publication No. SLAC-226, uc-28, (A), 1979 (unpublished), Stanford Linear Accelerator Center, Stanford University, Stanford, CA 94305. The gun employs cylindrical apertures and the design takes space charge into account.

[19] M. R. McMillan and J. H. Moore, Rev. Sci. Instrum. **51**, 944 (1980).

[20] In the initial design and construction, we had sharply truncated fields which were as uniform as possible up to the edge of the merger or demerger and which then rapidly dropped to zero. In practice and in more careful modeling, this was found to exacerbate beam shear, whereas natural fringe fields somewhat mitigate beam shear effects. Fringe fields were thus restored to the functioning device.

[21] Galileo Electro Optics, Type MCP 115. This information is provided for technical completeness and not as a product or company endorsement.

[22] The resistive anode was specially made for us for use with the rectangular microchannel plates by Surface Science Laboratories according to the prescription found in M. Lampton and C. W. Carlson, Rev. Sci. Instrum. **50**, 1093 (1979). This information is provided for technical completeness and not as a product or company endorsement.

[23] Surface Science Laboratories Model 2401. This information is provided for technical completeness and not as a product or company endorsement.

[24] D. A. Dahl and J. E. Delmore, SIMION, Technical Report No. EGG-CS-7233, Rev. 2, 1988 (unpublished), Idaho National Engineering Laboratory, EG&G Idaho Inc., P.O. Box 1625, Idaho Falls, ID 83415.

[25] T. Weiland, MAFIA (Release 3.1) manual, 1991, CST Ohlystrasse 69, D-6100 Darmstadt, Federal Republic of Germany. This information is provided for technical completeness and not as a product or company endorsment.

[26] Hewlett Packard Model HP340C+. This information is provided for technical completeness and not as a product or company endorsement.

[27] J. L. Wiza, Nucl. Instrum. Methods **162**, 587 (1979).

[28] Uncertainties are presented as per the guidelines in B. N. Taylor and C. E. Kuyatt, NIST Technical Note No. 1297, 1993 (unpublished).

[29] D. C. Griffin, N. R. Badnell, and M. S. Pindzola (private communication).

[30] N. H. Magee, Jr., J. B. Mann, A. L. Merts, and W. D. Robb, Report No. LA-8267-MS, Los Alamos Sci. Lab. (1977) (unpublished).

[31] S. T. Manson, Phys. Lett. **23**, 315 (1966).

[32] K. T. Chung (private communication).

[33] R. F. Welton, T. F. Morgan, and E. W. Thomas, J. Phys. B **24**, 3815 (1991).

[34] Peaked at $\theta=0°$, half height at $\theta=34°$ resulting from a partial-wave construction including partial waves only up to $l=2$. C. Bottcher (private communication).

[35] R. E. H. Clark (private communication).

[36] B. A. Huber, C. Ristori, R. A. Hervieux, M. Maurel, and H. J. Andrä, Phys. Rev. Lett. **67**, 1407 (1991); C. Ristori, R. A. Hervieux, M. Maurel, H. J. Andrä, A. Bernac, J. Crancon, G. Lamboley, Th. Lamy, Pl Perrin, J. C. Rocco, F. Zadworny, and B. A. Huber, Z. Phys. D **22**, 425 (1991).

[37] M. Lampton and J. Bixler, Rev. Sci. Instrum. **56**, 164 (1985).